View metadata, citation and similar papers at core.ac.uk
brought to you by CORE
provided by CiteSeerX

Proceedings of IMECE2006
2006 ASME International Mechanical Engineering Congress and Exposition
November 5-10, 2006, Chicago, Illinois, USA

IMECE2006-13668

NUMERICAL SIMULATIONS OF UNSTEADY FLUID FLOW AND HEAT TRANSFER IN A TRANSONIC TURBINE STAGE

F. Mumic
Division of Heat Transfer
Lund Institute of Technology
Box 118
22100 Lund, Sweden

B. Sunden
Division of Heat Transfer
Lund Institute of Technology
Box 118
22100 Lund, Sweden

ABSTRACT

In this work, a numerical study has been performed to simulate the unsteady fluid flow and heat transfer in a transonic high-pressure turbine stage. The main objective of this study is to understand the unsteady flow field and heat transfer in a single transonic turbine stage using an unsteady structured Navier-Stokes solver. For the time accurate computation, a fully implicit time discretization, dual-time stepping, is performed. The results of the CFD simulations are compared with experimental heat transfer and aerodynamic results available for the so-called MT1 turbine stage. The predicted heat transfer and static pressure distributions show reasonable agreement with experimental data. In particular, the results show significant fluctuations in heat transfer and pressure at mid-span on the rotor blade, and that the rotor has a limited influence on the heat transfer to the NGV at mid span.

INTRODUCTION

The flow field in a high pressure gas turbine is very complex. It is strongly three-dimensional, unsteady, viscous, with several types of secondary flows and vortices (passage vortex, leakage flow, horseshoe vortex, etc.). Transitional flow and high turbulence intensity result in additional complexities. The most significant contribution to the unsteadiness of the flow field is the relative motion of the blade rows. The understanding of such complex flow fields and the heat transfer characteristics is necessary to improve the blade design and prediction in terms of efficiency as well as the evaluation of mechanical and thermal fatigue. In the past decade computational fluid dynamics (CFD) have started to play an increasingly important role in the study of turbine blade for both flow and heat transfer. The advantage of using CFD for turbine heat transfer predictions is that the heat transfer in regions of complex flow fields (secondary flows, leakage flow, rotation, film cooling, stagnation point, etc.) can be reasonably determined, and that the heat transfer solution can also be obtained decently over the major turbine blade passage, including the hub, casing, and blade tip.

While the unsteadiness plays an important role in the flow through turbomachinery blade rows, the majority of flow simulations have been carried out as steady flow approximations. The inlet flow pattern is prescribed as uniform and steady. The main reasons for the lack of the unsteady numerical results are the large computational requirements necessary to calculate the flow solution and the long integration times to achieve meaningful time average. The most active area of unsteady turbomachinery research involves study on the influence of the unsteadiness on blade aerodynamic performance. A basic assessment considering the research activity and main impact of unsteady phenomena was given by Sharma et al. [1]. Examples of current unsteady, multi-stage turbomachinery flow prediction procedures include those of Arnone et al. [2], Ralf et al. [3], Martin and Alexander [4], Daniel et al. [5], Adami et al. [6,7], He et al. [8,9], Chana et al. [10], etc. One of the earliest works in this field is the simulation done by Arnone et al. [2]. They used a Navier-Stokes time-accurate solver and a four-stage Runge Kutte scheme to the analysis of unsteady rotor stator interaction. In a recent work by Denos et al. [11], numerical and experimental results of a transonic turbine stage are analyzed to understand how these non-uniformities are transported across the rotor. It is demonstrated that the vane shock is able to impose total pressure variation downstream of the stage that are large than that caused by the vane wakes. Abhari et al. [12] reported the results of a combined experimental and computational program that used the full-stage Rolls Royce ACE HPT stage operating at design corrected conditions. They found reasonably good agreement between the predicted and measured unsteady heat transfer on the early portion of the pressure surface and for a good deal of the suction surface. They did not find good agreement at the stagnation region of the blade. Dunn et al. [13]

Copyright © 2006 by ASME

Downloaded From: https://proceedings.asmedigitalcollection.asme.org on 06/30/2019 Terms of Use: http://www.asme.org/about-asme/terms-of-use

measured both the unsteady surface pressure and the unsteady heat flux at selected locations on the pressure and suction surface of the blade HPT stage. These results illustrate that the results predicted by Abhari et al. [12] are consistent with the measurement of Dunn et al. [13].

The present study is a continuation of an earlier study by Mumic and Sunden [14,15], where a numerical study was performed to simulate the heat transfer and fluid flow in a transonic high-pressure turbine stage with tip clearance. The stator and rotor rows interact via a mixing plane. The focus was on turbine aerodynamics and heat transfer behavior at the mid-span location, and at the rotor tip and casing region.

In the present work, a numerical study has been performed to simulate the unsteady fluid flow and heat transfer in a transonic high-pressure turbine stator passage. The objective of this work is to characterize and understand the unsteady flow field and heat transfer in a single transonic turbine stage using an unsteady structured Navier-Stokes solver. For the time accurate computation, a fully implicit time discretization, dual-time stepping is performed. The results of CFD simulations are compared with experimental heat transfer and aerodynamic results available for the so-called MT1 turbine stage. The simulations are performed using the commercial software FLUENT.

NOMENCLATURE

a Speed of sound (m/s)
C True chord of the vane (m)
CFL Courant number
Cx Axial chord of the vane (m)
k Thermal conductivity of the air (W/mK), also turbulent kinetic energy (m^2/s^2)
L Turbulent length scale (m)
Ma Isentropic Mach number, $\mathrm{Ma} = \sqrt{\frac{2}{\gamma-1}\left(\left(\frac{P_{0,in}}{P_s}\right)^{\frac{\gamma-1}{\gamma}}-1\right)}$
NGV Nozzle Guide Vane
Nu Nusselt number, $\mathrm{Nu} = \frac{\dot{q}C}{k(T_o - T_w)}$
P_s Local static pressure (Pa)
P_{oin} Total pressure at the inlet (Pa)
$\dot{q}$ Heat flux (W/m^2)
T Turbulent time scale (s)
T Passing period (s)
T_w Wall temperature (K)
T_o Inlet total temperature (K)
u_i Velocity vector (m/s)
u_τ Friction velocity (m/s) $u_\tau = \sqrt{\tau_w/\rho}$
y Distance from wall (m)
y^+ Dimensionless distance from the wall, $y^+ = \rho u_\tau y/\mu$
ρ Gas density (kg/m^3)
μ Viscosity (kg/ms)
τ_w Shear stress (N/m^2)
ε Dissipation rate of turbulence (m^2/s^3)
γ Ratio of specific heats
ω Rotor rotational speed
$\Delta\theta_p$ Blade pitch angle

TURBULENCE MODELS

In this work the v^2-f model have been used. The $v^2 - f$ model, introduced by Durbin [16], is similar to the standard k-ε model, but incorporates near wall turbulence anisotropy and non-local pressure-strain effects. It is a general low-Reynolds number turbulence model and therefore does not need to make use of wall functions. The distinguishing feature of the $v^2 - f$ model is its use of the velocity scale, $\overline{v^2}$, instead of the turbulent kinetic energy, k, for evaluating the eddy viscosity. The $v^2 - f$ model is a four-equation model based on transports for the turbulence kinetic energy (k), its dissipation rate (ε), a velocity variance scale ($\overline{v^2}$), and an elliptic relaxation function (f), which are obtained from the following transport equations:

$$\frac{\partial(\rho k)}{\partial t} + \frac{\partial(\rho k u_i)}{\partial x_i} = P - \rho\varepsilon + \frac{\partial}{\partial x_j}\left[\left(\mu + \frac{\mu_t}{\sigma_k}\right)\frac{\partial k}{\partial x_j}\right] + S_k \qquad (1)$$

$$\frac{\partial(\rho\varepsilon)}{\partial t} + \frac{\partial(\rho\varepsilon u_i)}{\partial x_i} = \frac{\partial}{\partial x_j}\left[\left(\mu + \frac{\mu_t}{\sigma_\varepsilon}\right)\frac{\partial \varepsilon}{\partial x_j}\right] + \frac{C'_{\varepsilon 1}P - C_{\varepsilon 2}\rho\varepsilon}{T} + S_\varepsilon \qquad (2)$$

$$\frac{\partial}{\partial t}\left(\rho\overline{v^2}\right) + \frac{\partial}{\partial x_i}\left(\rho\overline{v^2}u_i\right) = \rho k f - 6\rho\overline{v^2}\frac{\varepsilon}{k} + \frac{\partial}{\partial x_j}\left[\left(\mu + \frac{\mu_t}{\sigma_k}\right)\frac{\partial\overline{v^2}}{\partial x_j}\right] + S_{\overline{v^2}} \qquad (3)$$

$$f - L^2\frac{\partial^2 f}{\partial x_j^2} = (C_1 - 1)\frac{\frac{2}{3} - \overline{v^2}/k}{T} + C_2\frac{P}{\rho k} + \frac{5\overline{v^2}/k}{T} + S_f \qquad (4)$$

where

$$P = 2\mu_t S^2,\ S^2 = S_{ij}S_{ij},\ S_{ij} = \frac{1}{2}\left(\frac{\partial u_i}{\partial x_j} + \frac{\partial u_j}{\partial x_i}\right) \qquad (5)$$

The turbulent time scale T and length scale L are defined by

$$T = \min\left[\max\left(\frac{k}{\varepsilon}, 6\sqrt{\frac{v}{\varepsilon}}\right), \frac{\alpha}{\sqrt{3}}\frac{k^{3/2}}{\overline{v^2}C_\mu\sqrt{2S^2}}\right] \qquad (6)$$

$$L = C_L\max\left[\min\left(\frac{k^{3/2}}{\varepsilon}, \frac{1}{\sqrt{3}}\frac{k^{3/2}}{\overline{v^2}C_\mu\sqrt{2S^2}}\right), C_\eta\left(\frac{v^3}{\varepsilon}\right)^{1/4}\right] \qquad (7)$$

The turbulent (eddy) viscosity is defined as:

$$\mu_t = \rho C_\mu \overline{v^2} T \qquad (8)$$

The model constants that appear in the equations are specified as:

Copyright © 2006 by ASME

Downloaded From: https://proceedings.asmedigitalcollection.asme.org on 06/30/2019 Terms of Use: http://www.asme.org/about-asme/terms-of-use

$$\alpha = 0.6,\ C_1 = 1.4,\ C_2 = 0.3,\ C_{\varepsilon 1} = 1.4,\ C_{\varepsilon 2} = 1.9,\ C_\eta = 70,$$
$$C_\mu = 0.22,\ C_L = 0.23,\ \sigma_k = 1.0,\ \sigma_\varepsilon = 1.3, \quad (9)$$
$$C'_{\varepsilon 1} = C_{\varepsilon 1}\left(1 + 0.045\sqrt{k/v^2}\right)$$

NUMERICAL DETAILS

The numerical simulations in this investigation have been performed using a commercially available finite volume based Navier-Stokes solver FLUENT [17]. The solutions are obtained by solving the compressible Reynolds-averaged Navier-Stokes equations using a finite volume method to discretize the equations. For the time accurate computation, a full implicit time discretization, dual time stepping is performed. The overall accuracy is of second order.

The three-dimensional experimental test case used for validation is a transonic, unshrouded, high-pressure (HP) research turbine, known as MT1. It has been extensively tested for heat transfer and aerodynamic performance at QinetiQ, as described by Chana and Hilditch [18]. The stage has 32 nozzle guide vanes (NGV) and 60 rotor blades. The running rotor tip gap at 9500 rpm is estimated to be 0.56 mm. The NGV axial chord length is 37.5 mm and the angular pitch is 11.25º.

The boundary conditions for the calculation were set according to test data. The fact that the NGV and rotors generally have different numbers of blades has been addressed by including more blade passages in the calculation. A ratio of one NGV blade to two rotor blades was used to approximate the stage configuration. With respect to the machine geometry, the rotor blade distance in the pitch-wise direction has been slightly reduced to accommodate the 1:2 stator:rotor configuration. At the inlet, a total temperature of 444.4 K and a total pressure of 461.5 kPa are specified. The turbulence intensity is 6 percent and the length scale is set to be about 3 percent of the vane axial chord. The inlet is placed at one axial chord length upstream the leading edge and the flow at this location is fairly insensitive to downstream effects. At the exit, which is placed 2 axial chord lengths downstream the trailing edge of the rotor blade, the static pressure was specified as 143.15 kPa, which gave an overall pressure ratio of 3.22 across the blade. These conditions correspond to a NGV exit isentropic Mach number of 0.98 and are based on values reported in the experiments by Chana and Hilditch [18]. No-slip condition and a uniform wall temperature at 330 K are applied at the NGV and 300 K at the rotor blade, hub and shroud surfaces.

The computational grid at the mid-span is depicted in Figure 1. These grids are then stacked in the span-wise direction to produce the full three-dimensional grid. The computational domain is divided into different blocks for good control of the grid. Each block uses a suitable structured grid like an O-grid around the blade to have an optimum grid distribution around the blade, a C-grid away from the blade and an H-grid at the inlet block and outlet blocks. In Figure 2, some regions of the grid are shown in detail. This grid consists of different blocks and has a relatively complex topology which gives it a high quality and avoids strongly skewed cells. In order to limit the computational time, the spatial resolution in radial direction was chosen to be coarse with only 5 grid points.

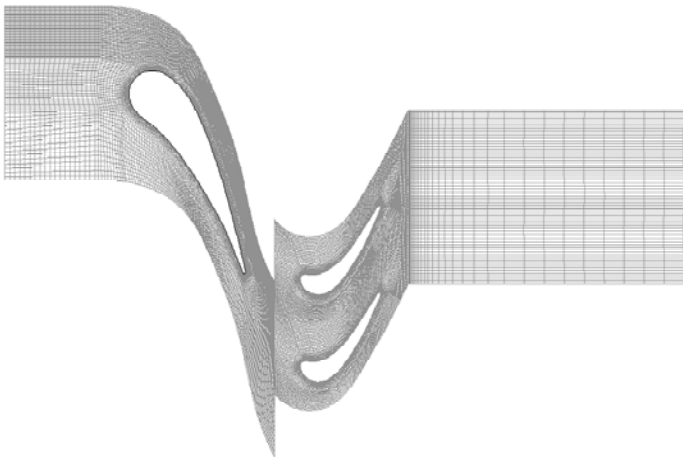

Figure 1. Computational domain and grids.

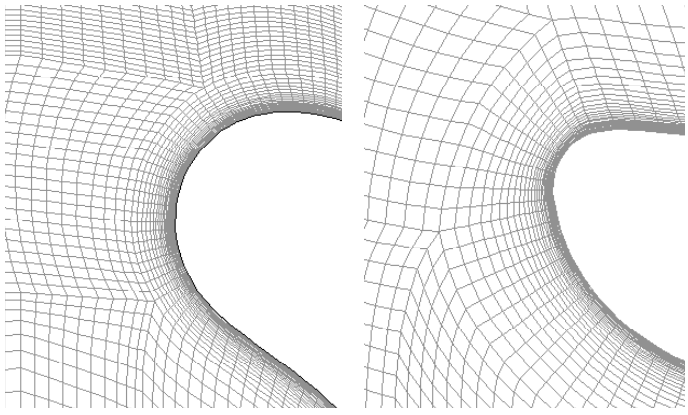

Figure 2. Some details of the computational grid.

The total number of cells was approximately 226,800. The y^+ values were in the range 0.2- 0.8.

All the cases presented have been converged to less than 0.001 percent mass flow error between the inlet and the exit of the computational domain. The heat transfer results have been checked for convergence by using heat transfer coefficient monitoring, and the solution was said to be converged when the

Copyright © 2006 by ASME

Downloaded From: https://proceedings.asmedigitalcollection.asme.org on 06/30/2019 Terms of Use: http://www.asme.org/about-asme/terms-of-use

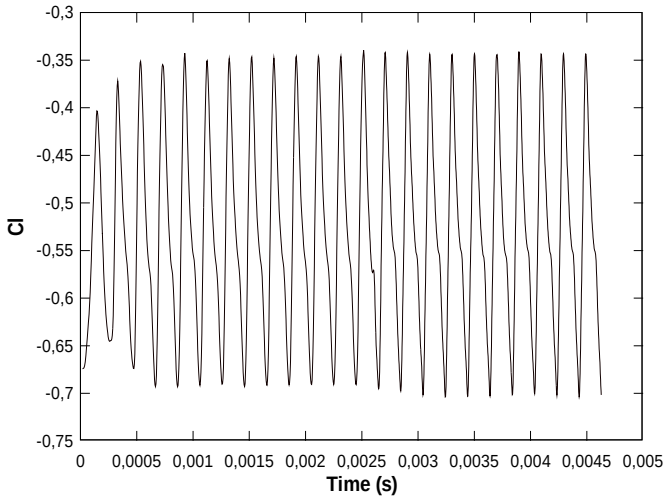

Figure 3. Lift coefficient history, moving rotor.

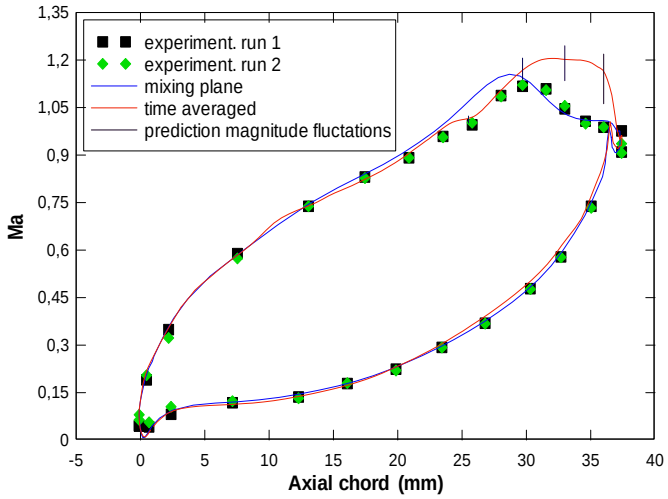

Figure 4. NGV mid-span isentropic Mach number distribution.

average heat transfer coefficient was not changed more than 0.01 W/m^{2}K during 10 successive iterations. The unsteady periodic solution has been reached starting from a steady state solution obtained at a fixed rotor position with respect to the stator. The flow becomes time periodic after about 16 passing period. The periodic response in the coefficients of lift is shown in Figure 3. The selection of the time-sep is critical for accurate time-dependent flow predictions. Here, the time step is chosen to be about 7.0x10^{-7} s and can be computed from

$$\Delta t = CFL\frac{\Delta x}{u+a} \tag{10}$$

where CFL is the Courant number, Δx is the local grid size, u is the local fluid velocity and a is the speed of the sound. The physical time, T, required to complete an entire period of the whole domain can be computed from

$$T = \frac{\Delta\theta_p}{\omega} = 1.97\times10^{-4}\,s \tag{11}$$

where $\Delta\theta_p$ is the blade pitch angle and ω is the rotor rotational speed. Using a time step of 7.0x10^{-7} s, 282 time steps will be performed as the rotor performs one pass. The numerical time marching convergence of each unsteady physical solution can be achieved within 90 numerical sub-iterations with a reduction of initial residuals large than 4 orders of magnitude.

RESULTS

The predicted and measured pressure fields of the vane are represented by the isentropic Mach numbers. The isentropic Mach number is defined as:

$$\mathrm{Ma} = \sqrt{\frac{2}{\gamma-1}\left(\left(\frac{P_{0,in}}{P_s}\right)^{\frac{\gamma-1}{\gamma}}-1\right)} \tag{12}$$

where $P_{0,in}$ is the total pressure at the inlet, P_s is the local static pressure and γ is the ratio of specific heats. A comparison

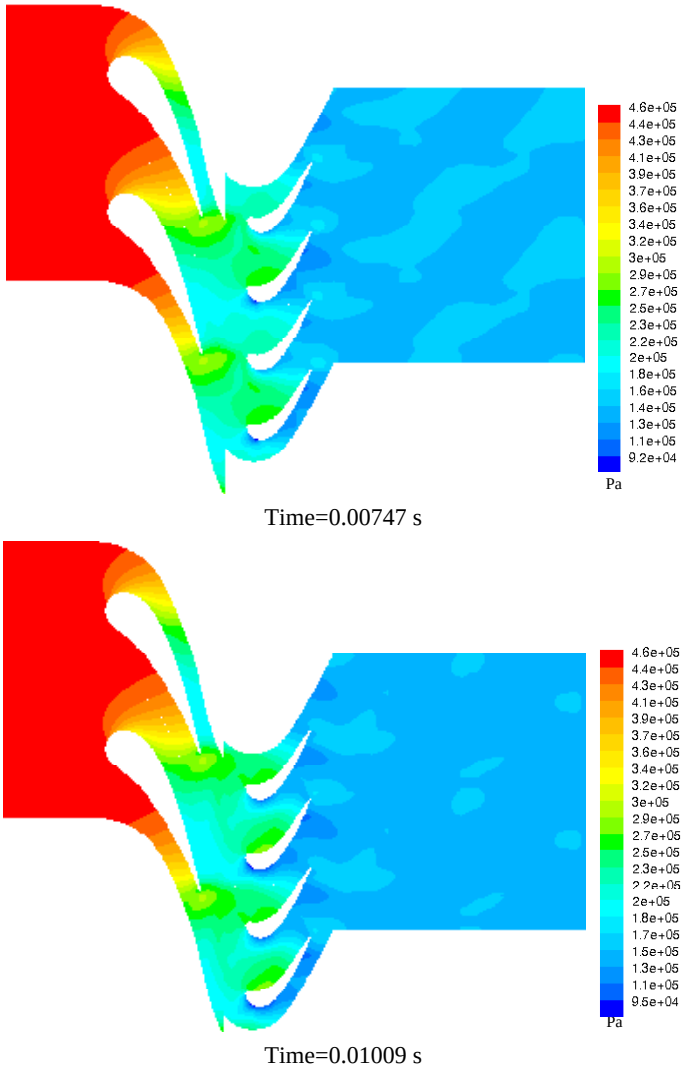

Figure 5. Contours of static pressure at two different times.

Copyright © 2006 by ASME

Downloaded From: https://proceedings.asmedigitalcollection.asme.org on 06/30/2019 Terms of Use: http://www.asme.org/about-asme/terms-of-use

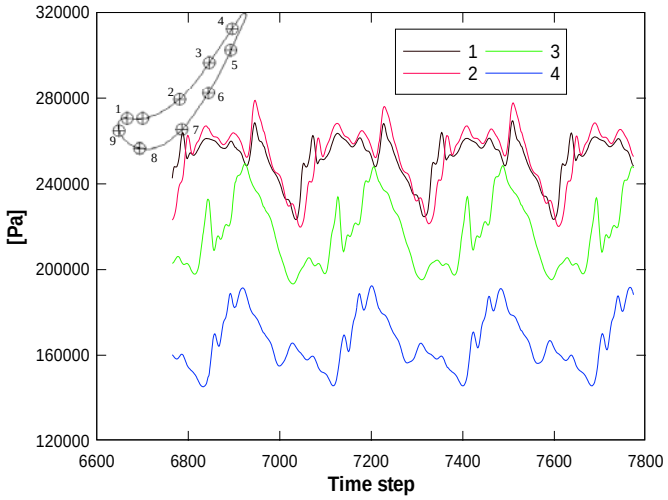

Figure 6. Unsteady static pressures at different chord-wise positions, rotor pressure surface.

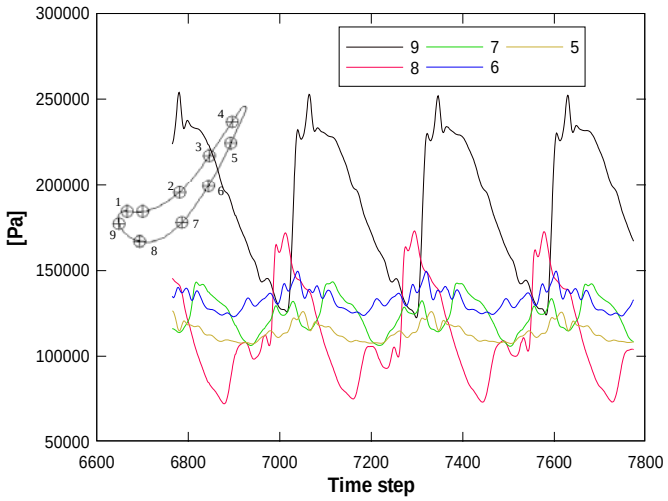

Figure 7. Unsteady static pressures at different chord-wise positions, rotor suction surface.

between the predicted steady [14] and unsteady and time averaged measured NGV blade surface isentropic Mach-number distributions at mid-span is shown in Figure 4. The predictions generally agree well with the experimental data, with the exception of the vane suction surface close to the trailing edge, where the predicted pressure is somewhat higher than the measurement, and the trailing edge shock from the unsteady solution hits the suction surface further downstream. The reason for this is unknown at this time; however, a possible explanation for this discrepancy is a difference in the back pressures between the solution operating conditions and the test conditions. The unsteady potential interaction between the NGV and rotor should mainly affect the region near the NGV trailing edge on the suction side, and this is the area where one can see a clear difference between the steady and unsteady solutions. The instantaneous view of the mid-span static pressure contours, shown in Figure 5 at two different time phases, clearly indicate that the pressure distribution around the

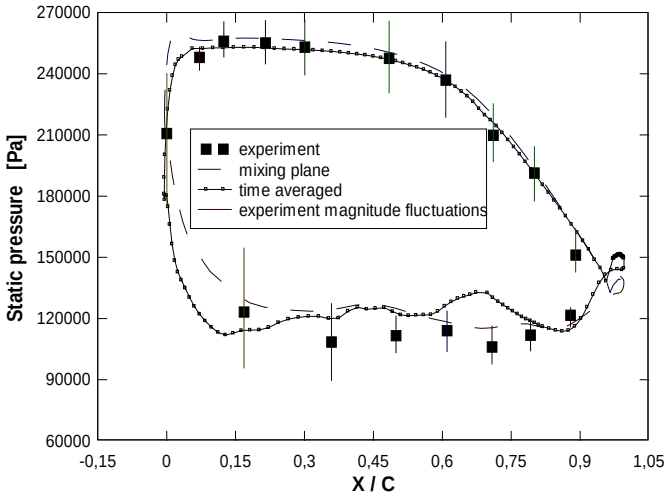

Figure 8. Rotor mid-span static pressure distribution.

leading edge of the rotor blade varies significantly from one time phase to another. The static pressure along the NGV varies in an observable magnitude only at the trailing edge on the suction side. It is also clearly seen that the static pressure decreases along the flow direction in the turbine stage since part of the total energy is converted to kinetic energy and transferred to the rotating blades as the fluid passes through the turbine stage.

Figures 6 and 7 show the predicted unsteady pressure fluctuations for the rotor at different chord-wise positions. The calculated time mean unsteady pressure variations are then compared with the experimental data and are shown in Figure 8. It is clear that the largest fluctuations are observed near the leading edge of the suction surface A maximum pressure amplitude of nearly 55 % of the inlet total pressure, and might be associated with the NGV trailing edge shock hitting the crown of the blade and sweeping the front suction side towards the leading edge, which is typical for transonic turbine stages. On the suction surface the fluctuations become smaller towards the trailing edge; the magnitude of the fluctuations is between 26 and 30% of the inlet total pressure, whereas on the pressure surface the fluctuations are greatest towards the trailing edge of the rotor, particularly at 40 and 80 % spans.

The predicted and experimental time-averaged pressure distributions around the rotor at mid-span are shown in Figure 8. Predicted steady (mixing-plane solution [14]) data are also plotted. The fluctuation amplitude is calculated as the difference between the maximum and minimum of the ensemble averaged signal, and is shown as a bar at each measurement location. The same good agreement between predictions and measurements was not possible to achieve for the rotor, as shown in Figure 8. The calculated surface pressures for the most of the suction surface are slightly higher than the experimental data. This can be an indication that the blade load is not identical with the experiments, perhaps an indication that the flow angles differ. It is also observed that the magnitude of the predicted fluctuations is higher than the measured ensemble average fluctuations. This is especially apparent on the suction surface. Very similar behaviour has been seen in other numerical predictions (e.g., Chana et al. [10]).

Copyright © 2006 by ASME

Downloaded From: https://proceedings.asmedigitalcollection.asme.org on 06/30/2019 Terms of Use: http://www.asme.org/about-asme/terms-of-use

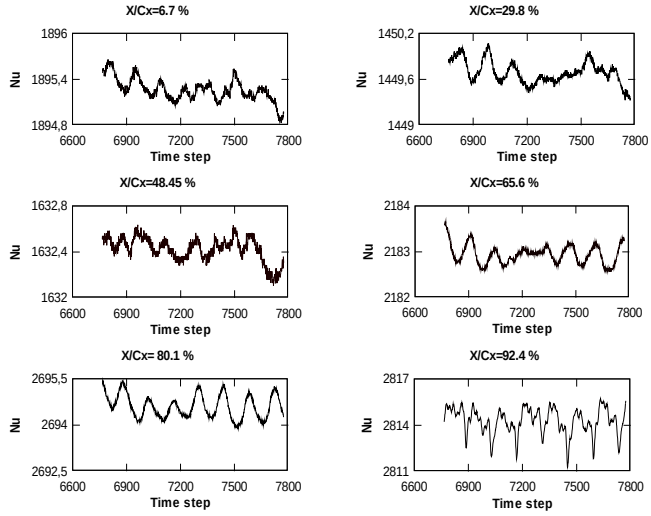

Figure 9. Unsteady heat transfer at different chord-wise positions, NGV pressure surface.

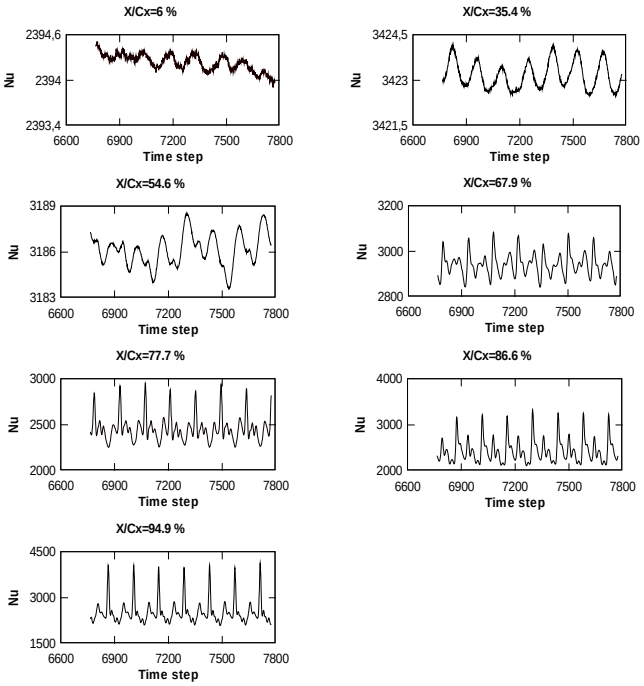

Figure 10. Unsteady heat transfer at different chord-wise positions, NGV suction surface.

After performing the aerodynamic computations, the heat transfer can be calculated in terms of a Nusselt number as:

$$Nu = \frac{\dot{q}C}{k(T_o - T_w)} \qquad (13)$$

Figures 9 and 10 show predicted heat transfer fluctuations for the NGV at six chord-wise locations on the pressure and at seven chord-wise locations on the suction surfaces of the NGV respectively (different ordinate scales have been used in these figures). The average magnitudes of the fluctuations were then

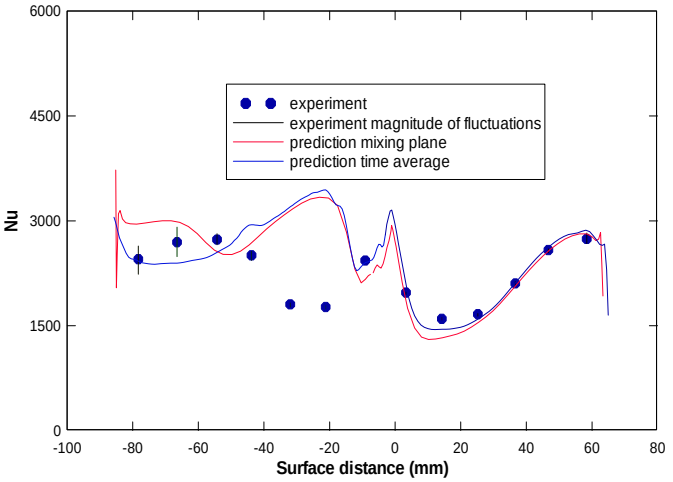

Figure 11. NGV mid-span Nusselt number distribution.

calculated and are shown in Figure 11. The fluctuations of a significant magnitude are only seen on the late suction surface and near the trailing edge on the pressure surface. This result was expected as the NGV is almost choked and hence much of the unsteadiness at the trailing edge is not able to propagate upstream beyond the throat. The average magnitude of the fluctuations superimposed on the mean Nusselt number is shown in Figure 11. Predicted steady (mixing-plane solution [14]) data are also plotted. The fluctuation amplitude is calculated as the difference between the maximum and minimum of the ensemble averaged signals and is shown as a bar at each measurement location. Again, the heat transfer along the NGV varies in an observable magnitude only at the near trailing edge on the pressure surface and on the late suction surface. Overall, the comparison between the unsteady solution and the experimental data for the NGV is very good on the pressure surface and on the suction surface near the trailing edge. Again, the trend is that calculations over-predict the unsteady magnitudes. This is especially apparent on the suction surface close to the leading edge, where the experimental results exhibit typical transitional behavior while the predictions don't capture this. Also, the unsteady result is closer to the experimental data than the steady mixing-plane solution.

Figures 12 and 13 show predicted heat transfer fluctuations for the rotor at five chord-wise locations on the pressure and at six chord-wise locations on the suction surfaces of the rotor, respectively. The average magnitudes of the fluctuations were then calculated and are shown in Figure 14. The largest fluctuations are observed in the leading edge region and significant fluctuations persist all along both surfaces. On the suction surface the lowest level of fluctuations can be seen at x/C_x= 79.8%. A comparison between the predicted unsteady and time averaged measured rotor blade surface Nusselt number distribution at mid-span is shown in Figure 14. Predicted steady (mixing-plane solution [14]) data are also plotted. The points represent the mean time averaged heat transfer level and the bars represent the fluctuation amplitude. Again, the fluctuation amplitude is calculated as the difference between the maximum and minimum of the ensemble average signals. It is again clearly seen that the fluctuations are largest near the leading edge, suction surface crown and the pressure surface trailing edge. Overall, the predicted heat transfer

Copyright © 2006 by ASME

Downloaded From: https://proceedings.asmedigitalcollection.asme.org on 06/30/2019 Terms of Use: http://www.asme.org/about-asme/terms-of-use

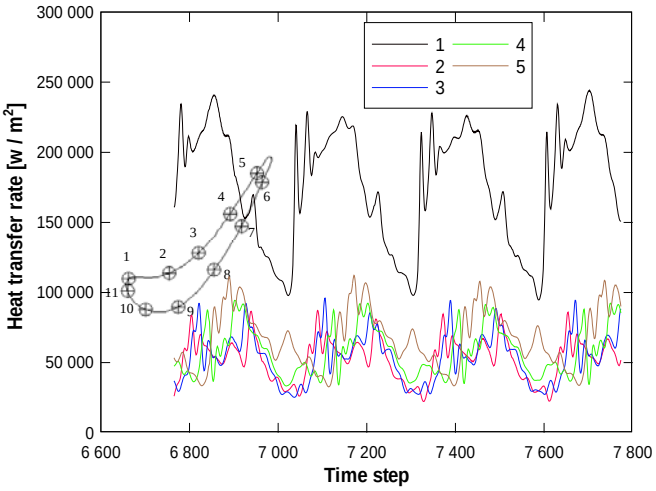

Figure 12. Unsteady heat transfer at different chord-wise positions, rotor pressure surface.

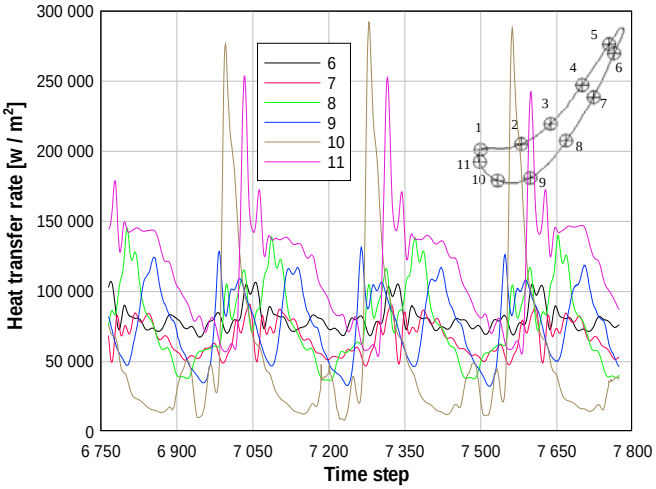

Figure 13. Unsteady heat transfer at different chord-wise positions, rotor suction surface.

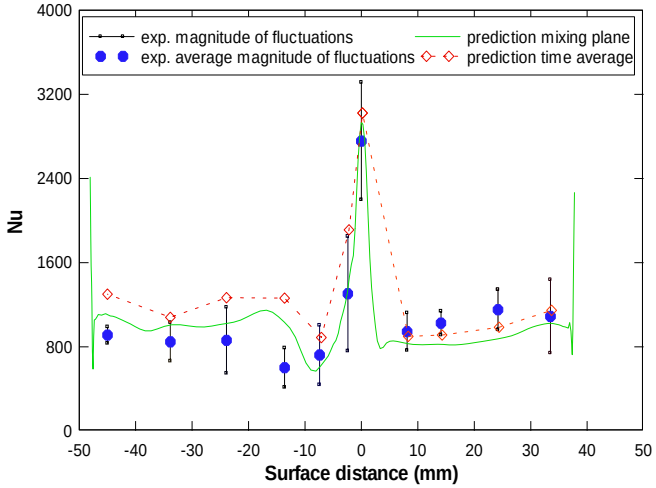

Figure 14. Rotor Nusselt number distribution at mid-span showing magnitude of fluctuations.

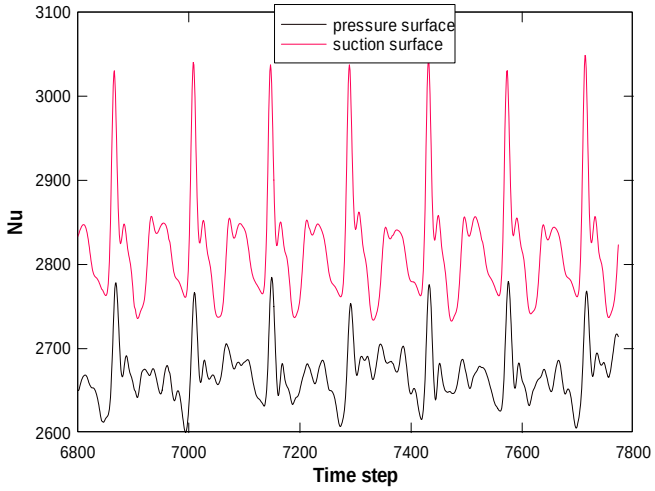

Figure 15. NGV mid-span average Nusselt number distribution.

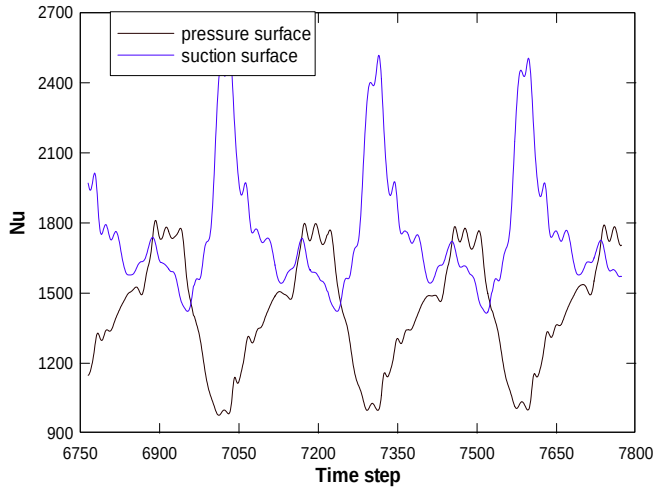

Figure 16. Rotor mid-span average Nusselt number distribution.

distributions show reasonable agreement with experimental data. In particular, the unsteady results show the trend to over-predict unsteady magnitude of the fluctuations. Nevertheless, the time-averaged unsteady calculation is somewhat closer to the experimental data on the pressure surface than the steady mixing-plane solution.

The periodic average heat transfer variation in terms of a Nusselt number for the NGV and rotor blade on all suction and pressure surfaces, at mid-span, are shown in Figures 15 and 16. As mentioned earlier, the largest fluctuations are observed on the rotor blade. It is clearly seen that the average heat transfer fluctuations are largest on the rotor suction surface. For the NGV, the fluctuations of an observable magnitude are only seen on the suction surface.

CONCLUSIONS

In the present study, numerical calculations have been performed to simulate the unsteady heat transfer and fluid flow in a transonic high-pressure turbine passage. The focus of this

Copyright © 2006 by ASME

Downloaded From: https://proceedings.asmedigitalcollection.asme.org on 06/30/2019 Terms of Use: http://www.asme.org/about-asme/terms-of-use

study is to characterize and understand the unsteady flow field and heat transfer in a single transonic turbine stage using an unsteady structured Navier-Stokes solver. For the time accurate computation, a fully implicit time discretization, dual-time stepping, is performed. The results of the CFD simulations are compared with experimental heat transfer and aerodynamic results available for the so-called MT1 turbine stage. The predicted heat transfer and static pressure distributions show reasonable agreement with experimental data.

The results show significant fluctuations in static pressure and heat transfer rate at mid-span on the rotor blade. The interaction of the NGV trailing edge shock with the rotor blade leads to extremely strong pressure gradients in the rotor leading-edge region and the front suction side with a maximum pressure amplitude of nearly 55 % of the inlet total pressure. Overall, it was found that the largest fluctuations of the heat transfer are observed on the rotor blade in the leading edge region and significant fluctuations persist all along both surfaces. For the NGV, the fluctuations of an observable magnitude are only found on the suction surface close to the trailing edge and near the trailing edge on the pressure surface. Overall, the predicted heat transfer distributions show reasonable agreement with experimental data. In particular, the unsteady results show the trend to over-predict unsteady magnitude of the fluctuations.

ACKNOWLEDGMENTS

This research is supported by Volvo Aero Corporation and the Swedish Energy Agency (STEM).

REFERENCES

[1] Sharma, O.P., Pickett, G.F., and Ni, R.H., 1990, "Assessment of Unsteady Flows in Turbines", ASME 90-GT-150.

[2] Arnone, A., and Pacciani, R., 1995, "Rotor-Stator Interaction Analysis Using the Navier-Stokes Equations and Multigrid Method" ASME GT-1995-117.

[3] Ralf, E.W., Heinz, E.G., Alexander, R.J., Jurgen, F.M., and Heinz, S., 1998, "Experimental and Computational Study of the Unsteady Flow in 1.5 Stage Axial Turbine with Emphasis on the Secondary Flow in the Second Stator", ASME GT-1998-254.

[4] Martin, V.H.H., and Alexander, R.J., 1999, "Comparison of Different Acceleration Techniques and Methods for Periodic Boundary Treatment in Unsteady Turbine Stage Flow Simulations", ASME GT-1999-155.

[5] Daniel, J.D., Lisa, W.G., and Frank, W.H., 2000, "A Study of the Effect of Tip Clearance in Supersonic Turbine", ASME GT-2000-447.

[6] Adami, P., Belardini, E., Martelli, F., and Michelassi, V., 2001, "Unsteady Rotor/Stator Interaction: an Improved Unstructured Aproach", ASME 2001-GT-0356.

[7] Ademi, P., Salvadori, S., and Shana, K.S., 2006, "Unsteady Heat Transfer Topics in Gas Turbine Stages Simulations", ASME GT-2006-90298.

[8] He, L., Menshikova, V., and Haller, B.R., 2004, "Influence of Hot Streak Circumferential Length-Scale in Transonic Turbine Stage", ASME GT-2004-53370.

[9] He, L., 2000, "Three Dimensional Unsteady Navier-Stokes Analysis of Stator-Rotor Interaction in Axial Flow Turbines", Part A, J. Power and Energy, Vol. 214, pp. 13-22.

[10] Chana, K.S., Singh, U.K and Povey, T., 2004, "Turbine Heat Transfer and Aerodynamic Measurements and Predictions for a 1.5 Stage Configuration", ASME GT2004-53951.

[11] Denos, R., Fidalgo, V.J., and Adami, P., 2006, "Transport of Unsteadiness across the Rotor of a Transonic Turbine Stage", ASME GT-2006-90462.

[12] Abhari, R.S., Guenette, G.R., Epstein, A.H., and Giles, M.B., 1991, "Comparison of Time-Resolved Turbine Rotor Blade Heat Transfer Measurements and Numerical Calculations", ASME 91-GT-268.

[13] Dunn, M.G., Haldeman, C.W., Abhari, R.S., and McMillan, M.L., 2000, "Influence of Vane/Blade Spacing on the Heat Flux for a Transonic Turbine", ASME J. Turbomachinery, Vol. 122, pp. 684-691.

[14] Mumic, F., and Sunden, B., 2006, "Numerical Prediction of Heat Transfer and Fluid Flow in a Transonic Turbine Stage", ICHMT Dubrovnik-Croatia.

[15] Mumic, F., and Sunden, B., 2006, "Effect of Free-Stream Turbulence on Heat Transfer and Fluid Flow in a Transonic Turbine Stage" IMECE2006-13669.

[16] Durbin, P.A., 1995, "Separated Flow Computations with the $k-\varepsilon-v^2$ Model", AIAA J. 33 (4), pp. 659-664.

[17] Fluent 6.1 User's Guide 2004.

[18] Chana, K.S., and Hilditch, M.A., 1995, "A Summary of Datum Uncooled Measurements of the MT1 Single Stage High Pressure Turbine in the DRA Pyestock Isentropic Light Piston Facility", IMT Area 3 Turbine Project, AER2-CT92-0044.

Copyright © 2006 by ASME

Downloaded From: https://proceedings.asmedigitalcollection.asme.org on 06/30/2019 Terms of Use: http://www.asme.org/about-asme/terms-of-use